Dietary Restriction Enhances CD8+ T Cell Ketolysis to Limit Exhaustion and Boost Anti-Tumor Immunity

Authors: Brandon M. Oswald[1], Lisa M. DeCamp[1], Joseph Longo[1], Michael S. Dahabieh[1], Nicholas Bunda[1], Shixin Ma[3], McLane J Watson[1], Ryan D. Sheldon[4], Michael P. Vincent[2,4], Benjamin K. Johnson[5], Abigail E Ellis[4], Molly T. Soper-Hopper[4], Christine N Isaguirre[4], Hui Shen[5], Kelsey S. Williams[1,2], Peter A. Crawford[6,7], Susan Kaech[3], H. Josh Jang[5], Connie M. Krawczyk[1,2], and Russell G. Jones[1,2]*

Affiliations:

[1]Department of Metabolism and Nutritional Programming, Van Andel Institute, Grand Rapids, MI, USA; [2]Metabolism and Nutrition (MeNu) Program, Van Andel Institute, Grand Rapids, MI, USA; [3]Salk Institute; [4]Mass Spectrometry Core Facility, Van Andel Institute, Grand Rapids, MI, USA; [5]Department of Epigenetics, Van Andel Institute, Grand Rapids, MI, USA; [6]Department of Medicine, Division of Molecular Medicine, University of Minnesota, Minneapolis, MN 55455, USA; [7]Department of Biochemistry, Molecular Biology, and Biophysics, University of Minnesota, Minneapolis, MN 55455, USA

*Corresponding author: Russell G. Jones, russell.jones@vai.org

Abstract

Reducing calorie intake without malnutrition limits tumor progression but the underlying mechanisms are poorly understood. Here we show that dietary restriction (DR) suppresses tumor growth by enhancing CD8$^+$ T cell-mediated anti-tumor immunity. DR reshapes CD8$^+$ T cell differentiation within the tumor microenvironment (TME), promoting the development of effector T cell subsets while limiting the accumulation of exhausted T (Tex) cells, and synergizes with anti-PD1 immunotherapy to restrict tumor growth. Mechanistically, DR enhances CD8$^+$ T cell metabolic fitness through increased ketone body oxidation (ketolysis), which boosts mitochondrial membrane potential and fuels tricarboxylic acid (TCA) cycle-dependent pathways essential for T cell function. T cells deficient for ketolysis exhibit reduced mitochondrial function, increased exhaustion, and fail to control tumor growth under DR conditions. Our findings reveal a critical role for the immune system in mediating the anti-tumor effects of DR, highlighting nutritional modulation of CD8$^+$ T cell fate in the TME as a critical determinant of anti-tumor immunity.

40   **Main Text**

41   **Introduction**

42   The balance between cancer cell proliferation and anti-tumor functions of the immune

43   system influences tumor growth (*1*). Immune checkpoint inhibitors (ICIs) have

44   revolutionized the treatment landscape for various malignancies in part by promoting

45   the expansion of CD8+ T cell subsets critical for controlling tumor progression (*2*). Given

46   their central role in mediating anti-tumor immunity, CD8+ T cells are often the target of

47   immune evasion and suppression mechanisms. Chronic exposure to tumor antigens

48   and inflammatory conditions in the tumor microenvironment (TME) can lead to CD8+ T

49   cell dysfunction (also known as exhaustion), a terminally differentiated state

50   characterized by reduced proliferative capacity and the expression of inhibitory

51   receptors (i.e., PD1, LAG3, TIM3) that limit T cell effector function (*3*, *4*). The

52   accumulation of exhausted T (Tex) cells in tumors is driven by the transcription factor

53   Thymocyte Selection-Associated High Mobility Group Box (TOX) and is reinforced

54   through epigenetic programming (*5–8*), this ultimately limits the ability of CD8+ T cells to

55   control tumor growth. Understanding mechanisms that drive CD8+ T cell fate decisions

56   in the TME is critical for developing new approaches to counter T cell dysfunction and

57   overcome ICI resistance during tumor progression.

58   T cell dysfunction is also influenced by environmental conditions in the TME that

59   impact T cell metabolism (*9, 10*). CD8+ T cells rely on glycolysis and oxidative

60   phosphorylation (OXPHOS) to fuel their proliferation and effector function (*11–13*).

61   Chronic antigen stimulation, hypoxic stress, and PD1 signaling all promote metabolic

62   and mitochondrial derangements in CD8+ T cells that precede their dysfunction (*14–17*).

63   Conversely, CD8^{+} T cell effector function is enhanced by exposure to nutrients that fuel

64   mitochondrial oxidative metabolism and acetyl-CoA levels, including ketone bodies

65   (KBs) and acetate (*18–20*). Nutrient levels in the TME are highly influenced by diet (*21*).

66   Thus, using dietary strategies that modulate metabolic conditions in the TME has the

67   potential to stimulate robust anti-tumor immunity, either in isolation or in combination

68   with ICI treatments, via metabolic enhancement of CD8^{+} T cell function.

69   Dietary restriction (DR), a regimen that reduces caloric intake without

70   malnutrition, extends lifespan in mammals and delays the onset of age-related diseases

71   including cancer (*22–26*). Dietary interventions that limit tumor growth—such as DR,

72   fasting-mimicking diets, or low glycemic diets—are presumed to act by altering the

73   levels of hormone (i.e., insulin, IGF-1) and/or metabolites (i.e., glucose) in the TME (*27–*

74   *30*). However, DR also exerts major effects on immune function (*31*). Despite lower

75   calorie intake, DR enhances both primary and memory T cell responses to bacterial

76   infection in mice (*32, 33*). Similarly, a 30% reduction in calorie intake is sufficient to

77   boost the proliferation and effector function of human T cells (*34*). Yet, the contribution

78   of the immune system to the anti-tumor effects of DR are unknown. Here, we show that

79   DR-driven changes in ketone body (KB) metabolism reshape CD8^{+} T fate in the TME to

80   control tumor growth.

81

82   **Results**

83   **Dietary restriction (DR) enhances T cell-mediated anti-tumor immunity**

84   To explore how the immune system contributes to the anti-tumor effects of DR, we

85   examined tumor growth in immunocompetent mice using an established model of DR

86   where daily food availability is reduced by 50% with no change to nutritional content

87   (**Table S1**) (*33*). C57BL/6J mice were fed either *ad libitum* (AL) or subjected to 50% DR

88   for 7 days prior to establishment of subcutaneous syngeneic tumor allografts (**Fig. 1a**).

89   Immune profiling revealed no change in $CD4^+$ T cell and NK cell populations but

90   increased numbers of $CD8^+$ T cells, eosinophils, and neutrophils in the spleen of DR-

91   conditioned mice compared to AL-fed controls after 1 week on the diet (**Table S2**). Mice

92   on the DR regimen displayed normal levels of physical activity (**Fig. S1a**) but consumed

93   50% less food and water on average (**Fig. 1b**, **S1b**), resulting in a ~15-20% loss in body

94   weight compared to AL-fed animals (**Fig. 1c**, **S1c**). Despite this weight loss, syngeneic

95   melanoma (B16) and breast cancer (E0771) tumors grew more slowly in mice adapted

96   to DR, corresponding to a 30-80% extension in tumor-free survival (**Fig. 1d-e**). These

97   results from DR are comparable to the delay in tumor growth observed in animals fed a

98   fasting-mimicking diet (FMD) (*35*). To interrogate the involvement of the immune system

99   in the anti-tumor effects of DR, we first assessed B16 melanoma tumor growth in $Rag2^{-/-}$

100   mice that lack mature T and B cells. Strikingly, the delay in tumor growth promoted by

101   DR was lost in *Rag2*-deficient animals (**Fig. 1f**). Similarly, there was no difference in

102   B16 tumor growth in athymic nude mice (that lack mature T cells) fed AL versus the DR

103   diet (**Fig. S2a**). Finally, depleting $CD8^+$ T cells accelerated B16 tumor growth under AL

104   conditions but also eliminated the tumor-delaying effects of DR (**Fig. 1g, S2b**).

105   Together, these data establish that DR limits tumor growth by promoting anti-tumor

106    $CD8^+$ T cell responses.

107   To determine how DR impacts immune cells in the TME, we performed cellular

108   indexing of transcriptomes and epitopes coupled to next generation sequencing (CITE-

109   seq) on live $CD45^+$ cells sorted from B16 tumors from AL- or DR-fed mice. This analysis

110   identified several cell clusters that categorized into three main groups: myeloid cells, T

111   cells, and NK cells (**Fig. 1h, S3a-b; Table S3**). The proportion of tumor-infiltrating T

112   cells (of $CD45^+$ cells) increased under DR, marked by an increase in $Gzmb^+$ $CD8^+$ T

113   effector (Teff) cells (**Fig 1h, S3c**). Histological analysis confirmed this increase in $CD8^+$

114   T cell infiltration into B16 tumors under DR conditions (**Fig. 1i, S3d**). The proportion of

115   myeloid cells in B16 tumors also changed in DR-fed mice, marked by a decrease in the

116   proportion of immunosuppressive $C1q^+$ tumor-associated macrophages (TAM) and an

117   expansion of $Ly6C^+$ inflammatory monocytes (**Fig 1h, S3e**). While recent work suggests

118   that DR can boost natural killer (NK) cell-mediated anti-tumor immunity (*36*), tumor-

119   infiltrating NK cell populations were similar between dietary conditions (**Fig. 1h**).

120   Overcoming resistance to immune checkpoint inhibitors (ICIs) is a major

121   challenge for cancer treatment. Given that DR enhances T cell-mediated control of

122   tumor growth, we tested the efficacy of combining DR with anti-PD1 immunotherapy in

123   mice bearing B16 melanoma tumors, which display resistance to PD1 blockade (*37*). *Ad*

124   *libitum* or DR-fed C57BL/6 mice were administered anti-PD1 or IgG control antibodies

125   beginning once tumors were palpable (~7 days post implantation). DR synergized with

126   anti-PD1 treatment, significantly extending the tumor-free survival of animals over anti-

127   PD1 treatment (under AL feeding) or DR treatment alone (**Fig. 1j**). Strikingly, ~15% of

128   animals treated with DR plus anti-PD1 immunotherapy remained tumor-free after 80

129   days (**Fig. 1j**). Thus, DR enhances the efficacy of ICI treatment even in tumors

130   refractory to conventional immunotherapies.

131

Dietary restriction reduces T cell dysfunction in the tumor microenvironment

Our data point to DR affecting CD8$^+$ T cell populations in the tumor microenvironment (TME). Thus, we used our CITE-seq datasets to characterize how DR impacts CD8$^+$ tumor infiltrating lymphocyte (TIL) populations. Cell clusters were classified based on gene features, gene density, antibody-derived tags (ADTs), and MSigDB pathway analysis (**Fig. S4a**). Cellular indexing of both protein epitopes and transcriptional profiling revealed two major CD8$^+$ TIL populations in B16 tumors based on gene expression for *Tox*, a key transcriptional regulator of T cell exhaustion (*5*, *6*) (**Fig. 2a**). The *Tox*^{Low} population consisted of five main subclusters including two *Mki67*$^+$ proliferating Teff cell populations (Prolif1 and Prolif2), two progenitor exhausted T cell populations (Tex^{Prog1}, Tex^{Prog2}), an intermediate exhausted (Tex^{Int}) population, and a small naïve-like cell population (**Fig. 2a**, **Fig. S4a-c**). *Tox*^{High} CD8$^+$ T cells displayed elevated transcript levels for inhibitory receptor genes (*Lag3*$^+$*Havcr2*$^+$*Pcdc1*$^+$), but clustered into two distinct groups: a conventional terminally exhausted (Tex^{Term}) population and a proliferating (*Mki67*$^+$) effector-like exhausted population (Tex^{Eff}) (**Fig. 2a-b**, **Fig. S4a-c**) (*3*). Fast Gene Set Enrichment Analysis (FGSEA) identified the Tex^{Eff} cluster as having the most effector-like properties, including enrichment for immune response and cell cycle genes (**Fig. 2b**). Tex^{Eff} cells also displayed increased expression of genes encoding effector molecules (i.e., *Ifng*, *Tnfa*, and *Gzmb*) (**Fig. 2b**), despite elevated expression of transcripts encoding *Tox* and inhibitory receptors (i.e., *Pdcd1*, *Lag3*, *Havcr2*) (**Fig. S4a**).

Single cell hashtagging strategies allowed us to track CD8$^+$ TIL populations in B16 tumors from either AL- or DR-fed mice. Analysis of CD8$^+$ TIL populations revealed

155   two major trends induced by DR feeding. First, for the Tox^{Low} CD8$^+$ TIL subset we

156   observed an expansion in proliferating effector T cell populations (Prolif1, Prolif2) and a

157   decrease in Tex^{Int} cells in animals conditioned to DR (**Fig. 2c-d**). Second, the type of

158   Tox^{High} Tex cells found in tumors was highly dependent on diet. Tumors from AL-fed

159   mice contained more terminally exhausted (Tex^{Term}) CD8$^+$ T cells, while tumors from DR

160   mice contained a greater proportion of effector-like cells (Tex^{Eff}) (**Fig. 2c-d**). To

161   determine whether the diet-induced changes in Tex cell populations reflect differences

162   in CD8$^+$ T cell differentiation, we employed RNA velocity analysis, a computational

163   method that infers cellular differentiation trajectories based on the abundance of spliced

164   and unspliced mRNA in single cells (*38*). Under AL conditions, RNA velocity pseudotime

165   (overlaid with velocity vectors) showed a directional flow away from the proliferating

166   effector population towards Tex^{Int} and ultimately Tex^{Term} populations (**Fig. 2e**). In

167   contrast, under DR the direction of CD8$^+$ T cell differentiation culminated in the effector-

168   like Tex^{Eff} population (**Fig. 2e**). This change in differentiation trajectory corresponded to

169   a major shift in the ratio of effector to terminally exhausted T cell populations in B16

170   tumors, moving from an equal effector to terminally exhausted ratio under AL-fed

171   conditions to a 4:1 ratio under DR (**Fig. S5a**). Collectively, these results indicate that

172   DR triggers a major shift in CD8$^+$ TIL fate away from terminal exhaustion towards a

173   more effector-like state that favors tumor control.

174   We next used flow cytometry to characterize the impact of DR on CD8 T cell

175   function within the TME. Consistent with our CITE-seq analysis, the number of CD8$^+$

176   Tex^{Term} cells—as determined by reduced TOX and inhibitory receptor (PD1$^+$TIM3$^+$)

177   expression—decreased significantly in tumors from DR-conditioned animals compared

178 to AL-fed mice 14 days post-tumor implantation (**Fig. 2f**). Using conventional markers

179 for terminally-exhausted (LY108⁻TIM3⁺) versus progenitor exhausted (LY108⁺TIM3⁻)

180 cells (*2*), the majority of PD1⁺ CD8 TIL in B16 tumors from DR-fed mice were progenitor

181 exhausted or an intermediate phenotype (LY108⁺TIM3⁺) (**Fig. S5b**) (*2*). In addition, the

182 percentage of effector CD8⁺ T cells (PD1^{low}TOX^{low}) was significantly increased under

183 DR (**Fig. 2f, S5c**) and these cells displayed increased features of stemness

184 (LY108/SLAMF6 expression, **Fig. S5d**) and cytotoxic function (Granzyme B production,

185 **Fig. S5e**). TOX-expressing CD8⁺ TILs from DR-fed mice displayed increased

186 expression of stemness markers (LY108/SLAMF6) and effector molecules (Granzyme

187 B), while showing reduced features of terminal exhaustion (i.e., lower PD1 and TOX

188 expression) compared to AL-fed controls (**Fig. 2g**). Thus, DR both enhances the

189 function and number of effector CD8⁺ T cells in the TME and promotes the accumulation

190 of TOX⁺ CD8⁺ T cells that are more stem-like, less exhausted, and functionally active.

191   Proliferative Tex cells expressing LY108/SLAMF6 are highly responsive to ICI

192 therapy (*2, 39, 40*). Given that DR synergizes with anti-PD1 treatment to slow tumor

193 growth (**Fig. 1j**), we investigated the impact of DR on anti-tumor CD8⁺ T cell populations

194 following ICI treatment. B16 tumor-bearing C57BL/6J mice subjected to DR were

195 administered either anti-PD1 or control IgG antibodies 7 days post-tumor implantation,

196 and CD8⁺ TIL phenotypes analyzed after 14 days of treatment (**Fig. S6**). Anti-PD1 ICI

197 therapy resulted in a ~3-fold decrease in TOX⁺PD1⁺ CD8⁺ TIL frequency (**Fig. 2h**).

198 Moreover, TOX-expressing CD8⁺ TILs were more functional following anti-PD1

199 treatment, marked by lower TOX expression and increased polyfunctionality (i.e., IFN-

200 γ^+TNF-α^+ and Granzyme B⁺ T cells) (**Fig. 2i**). Thus, anti-PD1 treatment amplifies the

201   effects of dietary restriction on CD8$^+$ T cell fate within the TME, favoring the expansion

202   of CD8$^+$ Teff and Tex^{Eff} cells.

203

204   **Dietary restriction enhances CD8$^+$ T cell metabolic fitness via ketone body**

205   **metabolism**

206   CD8$^+$ T cells are capable of metabolizing a diverse set of metabolic substrates to fuel

207   their growth and function (*18, 41, 42*). Given the impact of DR on CD8$^+$ T cell fate in the

208   TME, we assessed whether DR alters the metabolic programming of CD8$^+$ TIL subsets

209   that are important for tumor control. We first conducted metabolism-focused Gene Set

210   Enrichment Analysis (GSEA) on our CITE-seq datasets to define the metabolic features

211   of CD8$^+$ TIL subsets. This analysis revealed two distinct metabolically active CD8$^+$ TIL

212   populations in B16 tumors. CD8$^+$ T cells with effector properties (Prolif1, Tex^{Eff})

213   displayed the highest glycolytic signature (**Fig. 3a**), consistent with their high

214   proliferative rate (**Fig. 2a-b**). Notably, Tex^{Eff} cells⸺which preferentially expand in tumors

215   under DR (**Fig. 2c-d**)⸺displayed the highest OXPHOS signature of all CD8$^+$ TIL

216   subsets (**Fig. 3a**). Together, these results indicate that the most metabolically active

217   CD8$^+$ TIL subsets are the effector populations enhanced by DR treatment.

218   To evaluate how DR impacts CD8$^+$ Teff cell metabolism, we used a model of

219   *Listeria monocytogenes* (*Lm*) infection that elicits robust CD8$^+$ Teff cell responses in

220   vivo (*18, 43, 44*). Thy1.1$^+$ OT-I T cell receptor (TCR) transgenic CD8$^+$ T cells were

221   transferred into AL or DR-fed mice, followed by infection with attenuated *Listeria*

222   expressing ovalbumin (*Lm*OVA), and splenocytes extracted 7 days post infection (dpi)

223   for functional analysis (**Fig. S7a**). While OT-I CD8$^+$ T cells expanded less in DR-fed

224   mice (**Fig. S7b-d**), they displayed increased effector function, characterized by both an

225   increase in the percentage of IFN-γ-producing T cells (**Fig. S7e-f**) and higher IFN-γ

226   protein production on a per-cell basis (**Fig. S7g**). OT-I T cells from DR-treated animals

227   also displayed a ~2-fold increase in Granzyme B production (**Fig. S7h**). Metabolically,

228   OT-I Teff cells from DR mice displayed increased rates of oxygen consumption (**Fig.**

229   **3b**) and extracellular acidification (**Fig S8a**), corresponding to increased rates of ATP

230   production from both OXPHOS and glycolysis compared to CD8$^+$ T cells from AL-fed

231   animals (**Fig. 3c, S8b-c**). Consistent with increased mitochondrial metabolism, steady

232   state levels of TCA cycle-derived metabolites were elevated in DR-conditioned OT-I Teff

233   cells (**Fig. 3d, S8d**). In addition, both OT-I Teff cells responding to *Listeria* infection and

234   CD8$^+$ TILs isolated from B16 tumors displayed increased mitochondrial membrane

235   potential under DR conditions compared to CD8$^+$ T cells from AL-fed mice (**Fig. 3e**).

236   Together, these data indicate that DR boosts CD8$^+$ Teff cell bioenergetics, promoting

237   increased mitochondrial metabolism and OXPHOS.

238   Dietary modifications that alter systemic metabolism in mice can impact nutrient

239   availability in the TME (*21*, *27*, *45*). Thus, we hypothesized that DR impacts CD8$^+$ T cell

240   metabolism in part by altering the availability of specific nutrients in vivo. Indirect

241   calorimetry revealed that mice conditioned to DR displayed a significant decrease in

242   their respiratory exchange ratio (RER) during the fasted—but not the fed—state (**Fig.**

243   **S8e**), indicating increased lipid oxidation in DR-fed mice. We next used mass

244   spectrometry to profile diet-induced alterations in lipid and metabolite abundance in B16

245   tumors. We observed a general decrease in fatty acid and lipid abundance in DR

246   tumors compared to AL-fed controls (**Fig. 3f, S8f, Tables S5-6**). This change in tumor

247   lipid abundance is consistent with lipid mobilization from adipose tissue and a decrease

248   in respiratory exchange rate (RER) favoring oxidation triggered by DR (*27*, *33*) (**Fig.**

249   **S8e**). In contrast, only a small number of metabolites were enriched in tumors from DR-

250   treated mice, including increased abundance of the ketone β-hydroxybutyrate (βOHB)

251   (**Fig. 3f**). Elevated βOHB levels were observed in both tumors and serum from DR mice

252   compared to AL-fed mice (**Fig. 3g**).

253   The increase in circulating and intra-tumoral βOHB levels under DR was notable

254   given recent evidence linking ketone body (KB) metabolism to enhanced T cell effector

255   function (*19*, *46*). Using Seahorse bioenergetic analysis and ^{13}C-labeled metabolic

256   tracers, we found a striking difference in βOHB utilization by CD8$^+$ Teff cells based on

257   diet. First, augmenting DR-conditioned OT-I Teff cells with βOHB further increased their

258   maximal oxygen consumption rate (**Fig. 3h**). This change corresponds to a ~4-fold

259   increase in maximal oxidative ATP production capacity compared to Teff cells from AL-

260   fed animals (**Fig. 3h-i, S8h-g**). Next, we cultured OT-I Teff cells from *Lm*OVA-infected

261   mice ex vivo in physiologic medium (VIM) (*18*) containing fully-labeled [^{13}C$_6$]-glucose

262   and partially labelled [2,4-^{13}C$_2$]-βOHB. In this strategy, breakdown of [^{13}C$_6$]-glucose

263   generates M+2 labeled TCA cycle intermediates whereas [2,4-^{13}C$_2$]-βOHB generates

264   M+1 labeled intermediates (**Fig. 3j**), which thereby allowed us to directly compare the

265   contribution of each fuel type to TCA cycle metabolism (*19*). We observed a small but

266   significant increase in [^{13}C$_6$]-glucose-derived citrate (M+2) in DR-conditioned CD8$^+$ Teff

267   cells (**Fig. 3k, Table S7**); however, citrate labeling from [2,4-^{13}C$_2$]-βOHB (M+1) doubled

268   in CD8$^+$ Teff cells from DR compared to AL-fed mice (**Fig. 3l**). DR-conditioned OT-I Teff

269   cells also displayed a lower ratio of [2,4-^{13}C$_2$]-βOHB-labeled malate to citrate (**Fig. 3m**),

270 indicative of increased export of mitochondrial citrate to the cytosol (*47*). Consistent with

271 these observations, steady state acetyl-CoA levels were 2-fold higher in CD8$^+$ Teff cells

272 from DR mice relative to T cells from AL-fed controls (**Fig. 3n**). Thus, DR increases both

273 systemic βOHB availability and its utilization by CD8$^+$ T cells.

274

Ketone bodies fuel anti-tumor immunity under dietary restriction

276 One of the defining features of CD8$^+$ TILs from DR tumors is the expansion of

277 proliferating TOX$^+$ Tex cells with effector-like properties (Tex^{Eff} cells, **Fig. 2c-d**). To

278 better understand the metabolic properties of these cells, we analyzed transcriptional

279 profiles of CD8$^+$ TIL subsets from human tumors. Similar to CD8$^+$ TILs from mouse

280 tumors (**Fig. 2**), we identified CD8$^+$ effector T (Teff) cells and two exhausted (Tex) cell

281 clusters in TILs from human tumors (**Fig. 4a**). The dysfunctional or exhausted-like (Tex)

282 cell populations were distinguished from each other by the expression of the

283 proliferation marker *MKI67* (Tex^{Eff} versus Tex^{Term}, **Fig. S8i**). Tex^{Eff} cells from human

284 tumors most closely associated with Tex^{Eff} cluster of cells from mouse TILs (**Fig. 2a**).

285 Notably, both human Teff and Tex^{Eff} cells displayed significant increases in transcript

286 levels for βOHB dehydrogenase (*BDH1*), which encodes the rate-limiting enzyme

287 required for βOHB breakdown (**Fig. 4b**). Interestingly, proliferating Tex^{Eff} cells (human

288 TIL) displayed the highest ketone body metabolism gene signature of all human TIL

289 subsets (**Fig. 4c**), driven by increased expression of *BDH1* and 3-oxoacid CoA-

290 transferase 1 (*OXCT1*), which converts βOHB to acetoacetate (AcAc) (**Fig. 4b**).

291   In light of these findings, we assessed the metabolism of CD8$^+$ T cells exposed

292 to chronic antigenic stimulation that limits their self-renewal capacity and promotes

293   terminal differentiation (**Fig. S9a**) (*17*). Chronic stimulation of in vitro-activated CD8$^+$ T

294   cells with anti-CD3 and -CD28 antibodies promotes several features of T cell exhaustion

295   including increased expression of TOX and inhibitory receptors (i.e., PD1, TIM3) (**Fig.**

296   **S9b**), as well as reduced polyfunctionality (**Fig. S9c**) compared to activated CD8$^+$ T

297   cells maintained in IL-2 (acute stimulation). Surprisingly, chronically stimulated CD8$^+$ T

298   cells displayed increased abundance of TCA cycle intermediates compared to acutely

299   stimulated controls (**Fig. 4d**). This increase in TCA cycle intermediates was similar to

300   DR-conditioned CD8$^+$ T cells (**Fig. 3d**), leading us to hypothesize that chronic antigen

301   exposure may promote increased KB utilization. Using ^{13}C-βOHB as a metabolic tracer,

302   we found that chronically stimulated CD8$^+$ T cells displayed increased βOHB uptake

303   (**Fig. 4e, Table S8**) as well as higher βOHB oxidation in the TCA cycle as determined

304   by increased levels of ^{13}C-βOHB-derived citrate and malate compared to controls (**Fig.**

305   **4f, Table S8**). Chronically stimulated CD8$^+$ T cells also displayed a reduced malate-to-

306   citrate ratio (**Fig. 4g, Table S8**). This suggested a net export of βOHB-derived citrate to

307   the cytosol, similar to our observations for DR-conditioned T cells (**Fig. 3m**).

308   Collectively, these data suggest that chronic antigen exposure stimulates increased

309   βOHB uptake and metabolism by CD8$^+$ T cells.

310   Next, we assessed the contribution of βOHB metabolism by T cells to the anti-

311   tumor effects of DR. To test this, we generated mice with T cell-specific deletion of the

312   enzymes required to process KBs, βOHB dehydrogenase 1 (BDH1) and succinyl-

313   CoA:3-ketoacid CoA transferase (SCOT; encoded by *Oxct1*), by crossing *Cd4*^{Cre}

314   transgenic mice to mice with floxed alleles targeting the *Bdh1* and *Oxct1* genes

315   (Bdh1$^{fl/fl}$Oxct1$^{fl/fl}$*Cd4-Cre*, **Fig. S10a**). BDH1 mediates the conversion of βOHB to

316   acetoacetate (AcAc), while SCOT converts AcAc to acetoacetyl-CoA, ultimately leading

317   to the production of acetyl-CoA destined for the TCA cycle (**Fig. S10b**). Double

318   knockout (DKO) T cells (from *Bdh1*fl/fl*Oxct1*fl/fl*Cd4-Cre* mice) lacking both BDH1 and

319   SCOT were confirmed by immunoblot (**Fig. 4h**). Seahorse analysis of control (WT, from

320   Cre-negative *Bdh1*fl/fl*Oxct1*fl/fl mice) or DKO OT-I CD8$^+$ T cells isolated from *Lm*OVA-

321   infected mice demonstrated that loss of BDH1 and SCOT reversed the boost in

322   OXPHOS induced by DR feeding (**Fig. 4i, Fig. S10c-d**). Consistent with these

323   observations, DKO CD8$^+$ OT-I cells isolated from DR-fed mice displayed a significant

324   reduction in ^{13}C-βOHB labeling of TCA cycle intermediates (i.e., citrate, malate)

325   compared to controls (**Fig. 4j**). TMRM staining also revealed that the DR-induced

326   increase in mitochondrial membrane potential was blunted in DKO CD8$^+$ T cells (**Fig.**

327   **4k**). Together, these data indicate that T cell-intrinsic ketolysis is responsible for

328   maintaining T cell mitochondrial function and bioenergetic capacity under DR.

329   Finally, we assessed the contribution of T cell-intrinsic ketolysis to the anti-tumor

330   effects of DR by challenging control (WT) or DKO mice with syngeneic tumors. We

331   observed no difference in B16 melanoma tumor growth between DKO and control mice

332   under AL conditions; however, tumor growth was accelerated in DKO mice specifically

333   under DR conditions (**Fig. 4l**). Analysis of CD8$^+$ TIL from these mice revealed increases

334   in the accumulation of PD1$^+$TOX$^+$ Tex cells in the tumors of DR-fed DKO mice

335   compared to control animals (**Fig. 4m**). Furthermore, these DKO CD8$^+$ TIL maintained

336   high TOX levels even under DR feeding conditions (**Fig. 4n**). Together, these data link

337   T cell-intrinsic ketolysis to the anti-tumor effects of DR, with ketolysis deficient T cells

338   displaying increased features of exhaustion (i.e., TOX expression) in the TME.

339

340   **Discussion**

341   The tumor suppressive effects of reduced calorie intake have long been presumed to

342   act directly on cancer cells. Here, we demonstrate that dietary restriction (DR) works

343   more broadly to limit tumor growth by stimulating CD8$^+$ T cell anti-tumor immunity. We

344   show that DR alters CD8$^+$ T cell fate in the TME, promoting the expansion of tumor-

345   controlling effector (Teff-like and Tex^{Eff}) cells while limiting terminal T cell exhaustion.

346   Moreover, DR enhances CD8$^+$ T cell anti-tumor immunity by increasing circulating KB

347   levels, which in turn enhance TCA cycle metabolism and mitochondrial bioenergetics of

348   CD8$^+$ T cells. T cells that cannot metabolize KBs display metabolic deficits, undergo

349   premature exhaustion, and fail to control tumor growth under DR conditions, identifying

350   T cell-intrinsic ketolysis as a central mechanism for the anti-tumor effects of DR. These

351   findings, along with our previous research identifying ketolysis as a regulator of CD8$^+$ T

352   cell cytolytic function (*19, 46*), suggest that DR regulates a *nutrient-sensitive checkpoint*

353   within the TME—mediated by ketones—that promotes the expansion of tumor-

354   controlling effector (Teff-like and Tex^{Eff}) T cells over terminal exhaustion, thereby

355   improving tumor control. Overall, our study highlights how altering systemic nutrient

356   availability through diet can influence CD8$^+$ T cell fate within tumors to limit cancer

357   progression.

358   βOHB is preferentially oxidized over glucose for ATP production in CD8$^+$ T cells

359   and boosts T cell effector responses (*21, 48*). Our data indicate that βOHB uptake and

360   oxidation is a metabolic feature of T cells exposed to chronic stimulation. Increased

361   *BDH1* expression in CD8$^+$ T cells, which we observed in TILs from human tumors,

362 facilitates greater βOHB oxidation in TIL as they infiltrate solid tumors. Many tumors are

363 nutrient-poor (*19*). By increasing KB availability approximately fourfold compared to *ad*

364 *libitum*-fed conditions, DR boosts the available βOHB supply in the TME, fueling the

365 TCA cycle to meet the oxidative demands of CD8^{+} TIL. Consistent with this, CD8^{+} T

366 cells adapted to DR were found to display increased mitochondrial membrane potential

367 and oxidative ATP production. This metabolic advantage promotes the expansion of

368 Tex[Eff] cells, which retain proliferative capacity and effector function, over Tex[Term] cells

369 with high inhibitory receptor expression and diminished functionality. These metabolic

370 advantages are lost in ketolysis-deficient (DKO) T cells, contributing to their premature

371 exhaustion. Thus, DR aligns systemic nutrient supply with the metabolic needs of T

372 cells at the tissue level.

373   A critical metabolic fate of βOHB oxidation in CD8^{+} T cells is acetyl-CoA, the

374 levels of which double under DR-fed conditions. We have shown that βOHB is the major

375 substrate for acetyl-CoA production in CD8^{+} T cells under physiologic conditions (*49,*

376 *50*). The role of acetyl-CoA extends beyond biosynthetic growth (i.e., *de novo*

377 lipogenesis) and energy production: it is the rate-limiting substrate for histone

378 acetylation reactions that regulate T cell differentiation and effector function (*20*). Our

379 results here argue that nutritional regulation of KB metabolism is a critical determinant

380 of CD8^{+} T cell fate in the TME, shifting differentiation between terminally exhausted

381 (Tex[Term]) and effector-like (Tex[Eff]) states. Consistent with this, pantothenate/Coenzyme

382 A (CoA) increases CD8^{+} T cell differentiation towards effector lineages to enhance

383 tumor control (*51–53*). We speculate that, under DR, βOHB-dependent changes in

384 acetyl-CoA levels drive changes in T cell epigenetic programming favoring effector

385   responses over exhaustion. Thus, dietary interventions or therapeutics that boost

386   acetyl-CoA production in T cells may improve anti-tumor immunity similar to DR.

387   The mammalian immune system evolved under cyclical periods of feast and

388   famine. Immune challenges such as infection further impact systemic nutrient

389   availability by disrupting feeding behaviors and remodeling host metabolism (*54*, *55*).

390   Mobilizing stored energy from adipose tissue into KB production provides the host with

391   a versatile fuel to maintain acetyl-CoA production under conditions of metabolic stress

392   (*56*). In this vein, we speculate that T cells evolved the use of ketolysis to buffer against

393   metabolic perturbations that negatively impact T cell bioenergetics and function. Our

394   findings reveal the potential of exploiting this system through nutritional interventions

395   that enhance anti-tumor immunity. PD1 blockade amplifies the anti-tumor effects of DR

396   by promoting the expansion of effector T cells (Teff and Tex[Eff] cells) to limit tumor

397   growth, highlighting the potential of enhancing the efficacy of immunotherapies through

398   nutritional intervention. Employing DR in clinical settings may face challenges regarding

399   feasibility due to patient health and compliance. However, combining ICIs with

400   pharmacological agents that reduce appetite and food intake, such as GLP-1 agonists

401   like semaglutide (i.e., Ozempic), may mimic some metabolic effects of DR without

402   necessitating strict dietary regimens (*57*). Our findings also have potential implications

403   for adoptive T cell therapies, including chimeric antigen receptor (CAR) T-cell therapy.

404   The metabolic state of T cells prior to infusion is critical for their persistence,

405   functionality, and anti-tumor efficacy in patients (*45*). Exposing CAR T cells to a DR-like

406   environment during expansion or enhancing their capacity to oxidize KBs may improve

407   their metabolic fitness and resistance to terminal exhaustion *in vivo*, thereby increasing

408   their therapeutic efficacy.

409   One caveat of this work is that the chow used is relatively low-fat (15% of

410   calories from fat) compared to the standard western diet. High-fed feeding antagonizes

411   anti-tumor T cell responses (*58*); thus, it is crucial to dissect the impact of macronutrient

412   content, particularly carbohydrate and fats (*19*), on the anti-tumor effects of DR.

413   Understanding how dietary interventions such as DR impact T cell metabolism and

414   differentiation fate in the TME may lead to evidence-based nutritional guidelines that

415   complement and enhance cancer immunotherapy efforts.

416

References

1. D. Hanahan, R. A. Weinberg, Hallmarks of cancer: the next generation. *Cell* **144**, 646–674 (2011).

2. B. C. Miller, D. R. Sen, R. Al Abosy, K. Bi, Y. V. Virkud, M. W. LaFleur, K. B. Yates, A. Lako, K. Felt, G. S. Naik, M. Manos, E. Gjini, J. R. Kuchroo, J. J. Ishizuka, J. L. Collier, G. K. Griffin, S. Maleri, D. E. Comstock, S. A. Weiss, F. D. Brown, A. Panda, M. D. Zimmer, R. T. Manguso, F. S. Hodi, S. J. Rodig, A. H. Sharpe, W. N. Haining, Subsets of exhausted CD8+ T cells differentially mediate tumor control and respond to checkpoint blockade. *Nat. Immunol.*, doi: 10.1038/s41590-019-0312-6 (2019).

3. B. Daniel, K. E. Yost, S. Hsiung, K. Sandor, Y. Xia, Y. Qi, K. J. Hiam-Galvez, M. Black, C. J Raposo, Q. Shi, S. L. Meier, J. A. Belk, J. R. Giles, E. J. Wherry, H. Y. Chang, T. Egawa, A. T. Satpathy, Divergent clonal differentiation trajectories of T cell exhaustion. *Nat. Immunol.* **23**, 1614–1627 (2022).

4. L. M. McLane, M. S. Abdel-Hakeem, E. J. Wherry, CD8 T Cell Exhaustion During Chronic Viral Infection and Cancer. *Annu. Rev. Immunol.* **37**, 457–495 (2019).

5. O. Khan, J. R. Giles, S. McDonald, S. Manne, S. F. Ngiow, K. P. Patel, M. T. Werner, A. C. Huang, K. A. Alexander, J. E. Wu, J. Attanasio, P. Yan, S. M. George, B. Bengsch, R. P. Staupe, G. Donahue, W. Xu, R. K. Amaravadi, X. Xu, G. C. Karakousis, T. C. Mitchell, L. M. Schuchter, J. Kaye, S. L. Berger, E. J. Wherry, TOX transcriptionally and epigenetically programs CD8+ T cell exhaustion. *Nature*, doi: 10.1038/s41586-019-1325-x (2019).

6. C. Yao, H. W. Sun, N. E. Lacey, Y. Ji, E. A. Moseman, H. Y. Shih, E. F. Heuston, M. Kirby, S. Anderson, J. Cheng, O. Khan, R. Handon, J. Reilley, J. Fioravanti, J. Hu, S. Gossa, E. J. Wherry, L. Gattinoni, D. B. McGavern, J. J. O'Shea, P. L. Schwartzberg, T. Wu, Single-cell RNA-seq reveals TOX as a key regulator of CD8+ T cell persistence in chronic infection. *Nat. Immunol.* **20**, 890–901 (2019).

7. J. A. Belk, B. Daniel, A. T. Satpathy, Epigenetic regulation of T cell exhaustion. *Nat. Immunol.* **23**, 848–860 (2022).

8. D. R. Sen, J. Kaminski, R. A. Barnitz, M. Kurachi, U. Gerdemann, K. B. Yates, H. W. Tsao, J. Godec, M. W. LaFleur, F. D. Brown, P. Tonnerre, R. T. Chung, D. C. Tully, T. M. Allen, N. Frahm, G. M. Lauer, E. J. Wherry, N. Yosef, W. N. Haining, The epigenetic landscape of T cell exhaustion. *Science*, doi: 10.1126/science.aae0491 (2016).

9. D. G. Roy, I. Kaymak, K. S. Williams, E. H. Ma, R. G. Jones, Immunometabolism in the Tumor Microenvironment. *Annu. Rev. Cancer Biol.* **5**, 137–159 (2021).

10. A. R. Lim, W. K. Rathmell, J. C. Rathmell, The tumor microenvironment as a metabolic barrier to effector T cells and immunotherapy. *Elife* **9** (2020).

11. M. D. Buck, R. T. Sowell, S. M. Kaech, E. L. Pearce, Metabolic Instruction of Immunity. *Cell* **169**, 570–586 (2017).

12. Z. A. Bacigalupa, M. D. Landis, J. C. Rathmell, Nutrient inputs and social metabolic control of T cell fate. *Cell Metab.* **36**, 10–20 (2024).

13. N. M. Chapman, H. Chi, Metabolic adaptation of lymphocytes in immunity and disease. *Immunity* **55**, 14–30 (2022).

14. B. Bengsch, A. L. Johnson, M. Kurachi, P. M. Odorizzi, K. E. Pauken, J. Attanasio, E. Stelekati, L. M. McLane, M. A. Paley, G. M. Delgoffe, E. J. Wherry, Bioenergetic Insufficiencies Due to Metabolic Alterations Regulated by the Inhibitory Receptor PD-1 Are an Early Driver of CD8+ T Cell Exhaustion. *Immunity* **45**, 358–373 (2016).

15. N. E. Scharping, D. B. Rivadeneira, A. V. Menk, P. D. A. Vignali, B. R. Ford, N. L. Rittenhouse, R. Peralta, Y. Wang, Y. Wang, K. DePeaux, A. C. Poholek, G. M. Delgoffe, Mitochondrial stress induced by continuous stimulation under hypoxia rapidly drives T cell exhaustion. *Nat. Immunol.* **22**, 205–215 (2021).

16. Y.-R. Yu, H. Imrichova, H. Wang, T. Chao, Z. Xiao, M. Gao, M. Rincon-Restrepo, F. Franco, R. Genolet, W.-C. Cheng, C. Jandus, G. Coukos, Y.-F. Jiang, J. W. Locasale, A. Zippelius, P.-S. Liu, L. Tang, C. Bock, N. Vannini, P.-C. Ho, Disturbed mitochondrial dynamics in CD8+ TILs reinforce T cell exhaustion. *Nat. Immunol.* **21**, 1540–1551 (2020).

17. S. A. Vardhana, M. A. Hwee, M. Berisa, D. K. Wells, K. E. Yost, B. King, M. Smith, P. S. Herrera, H. Y. Chang, A. T. Satpathy, M. R. M. van den Brink, J. R. Cross, C. B. Thompson, Impaired mitochondrial oxidative phosphorylation limits the self-renewal of T cells exposed to persistent antigen. *Nat. Immunol.*, doi: 10.1038/s41590-020-0725-2 (2020).

18. I. Kaymak, K. M. Luda, L. R. Duimstra, E. H. Ma, J. Longo, M. S. Dahabieh, B. Faubert, B. M. Oswald, M. J. Watson, S. M. Kitchen-Goosen, L. M. DeCamp, S. E. Compton, Z. Fu, R. J. DeBerardinis, K. S. Williams, R. D. Sheldon, R. G. Jones, Carbon source availability drives nutrient utilization in CD8+ T cells. *Cell Metab.* **34**, 1298-1311.e6 (2022).

19. K. M. Luda, J. Longo, S. M. Kitchen-Goosen, L. R. Duimstra, E. H. Ma, M. J. Watson, B. M. Oswald, Z. Fu, Z. Madaj, A. Kupai, B. M. Dickson, L. M. DeCamp, M. S. Dahabieh, S. E. Compton, R. Teis, I. Kaymak, K. H. Lau, D. P. Kelly, P. Puchalska, K. S. Williams, C. M. Krawczyk, D. Lévesque, F.-M. Boisvert, R. D. Sheldon, S. B. Rothbart, P. A. Crawford, R. G. Jones, Ketolysis drives CD8+ T cell effector function through effects on histone acetylation. *Immunity* **56**, 2021-2035.e8 (2023).

20. M. St Paul, S. D. Saibil, S. Han, K. Israni-Winger, S. C. Lien, R. C. Laister, A. Sayad, S. Penny, R. N. Amaria, L. E. Haydu, C. R. Garcia-Batres, M. Kates, D. T. Mulder, C. Robert-Tissot, M. J. Gold, C. W. Tran, A. R. Elford, L. T. Nguyen, T. J.

Pugh, D. M. Pinto, J. A. Wargo, P. S. Ohashi, Coenzyme A fuels T cell anti-tumor immunity. *Cell Metab.* **33**, 2415-2427.e6 (2021).

21. M. R. Sullivan, L. V. Danai, C. A. Lewis, S. H. Chan, D. Y. Gui, T. Kunchok, E. A. Dennstedt, M. G. Vander Heiden, A. Muir, M. G. V. Heiden, A. Muir, Quantification of microenvironmental metabolites in murine cancers reveals determinants of tumor nutrient availability. *Elife* **8** (2019).

22. A. Nencioni, I. Caffa, S. Cortellino, V. D. Longo, Fasting and cancer: molecular mechanisms and clinical application. *Nat. Rev. Cancer* **18**, 707–719 (2018).

23. A. Mishra, G. Giuliani, V. D. Longo, Nutrition and dietary restrictions in cancer prevention. *Biochim. Biophys. Acta Rev. Cancer* **1879**, 189063 (2024).

24. S. D. Hursting, J. A. Lavigne, D. Berrigan, S. N. Perkins, J. C. Barrett, Calorie restriction, aging, and cancer prevention: mechanisms of action and applicability to humans. *Annu. Rev. Med.* **54**, 131–152 (2003).

25. D. Kritchevsky, Caloric restriction and cancer. *J. Nutr. Sci. Vitaminol. (Tokyo)* **47**, 13–19 (2001).

26. L. Fontana, L. Partridge, V. D. Longo, Extending healthy life span--from yeast to humans. *Science* **328**, 321–326 (2010).

27. E. C. Lien, A. M. Westermark, Y. Zhang, C. Yuan, Z. Li, A. N. Lau, K. M. Sapp, B. M. Wolpin, M. G. Vander Heiden, Low glycaemic diets alter lipid metabolism to influence tumour growth. *Nature* **599**, 302–307 (2021).

28. B. D. Hopkins, C. Pauli, D. Xing, D. G. Wang, X. Li, D. Wu, S. C. Amadiume, M. D. Goncalves, C. Hodakoski, M. R. Lundquist, R. Bareja, Y. Ma, E. M. Harris, A. Sboner, H. Beltran, M. A. Rubin, S. Mukherjee, L. C. Cantley, Suppression of insulin feedback enhances the efficacy of PI3K inhibitors. *Nature*, doi: 10.1038/s41586-018-0343-4 (2018).

29. N. Y. Kalaany, D. M. Sabatini, Tumours with PI3K activation are resistant to dietary restriction. *Nature* **458**, 725–731 (2009).

30. M. Wei, S. Brandhorst, M. Shelehchi, H. Mirzaei, C. W. Cheng, J. Budniak, S. Groshen, W. J. Mack, E. Guen, S. Di Biase, P. Cohen, T. E. Morgan, T. Dorff, K. Hong, A. Michalsen, A. Laviano, V. D. Longo, Fasting-mimicking diet and markers/risk factors for aging, diabetes, cancer, and cardiovascular disease. *Sci. Transl. Med.* **9** (2017).

31. N. Collins, Y. Belkaid, Control of immunity via nutritional interventions. *Immunity* **55**, 210–223 (2022).

32. C. Palma, C. La Rocca, V. Gigantino, G. Aquino, G. Piccaro, D. Di Silvestre, F. Brambilla, R. Rossi, F. Bonacina, M. T. Lepore, M. Audano, N. Mitro, G. Botti, S.

530 Bruzzaniti, C. Fusco, C. Procaccini, V. De Rosa, M. Galgani, C. Alviggi, A. Puca, F.
531 Grassi, T. Rezzonico-Jost, G. D. Norata, P. Mauri, M. G. Netea, P. de Candia, G.
532 Matarese, Caloric Restriction Promotes Immunometabolic Reprogramming Leading
533 to Protection from Tuberculosis. *Cell Metab.*, doi: 10.1016/j.cmet.2020.12.016
534 (2021).

535 33. N. Collins, S. J. Han, M. Enamorado, V. M. Link, B. Huang, E. A. Moseman, R. J.
536 Kishton, J. P. Shannon, D. Dixit, S. R. Schwab, H. D. Hickman, N. P. Restifo, D. B.
537 McGavern, P. L. Schwartzberg, Y. Belkaid, The Bone Marrow Protects and
538 Optimizes Immunological Memory during Dietary Restriction. *Cell*, doi:
539 10.1016/j.cell.2019.07.049 (2019).

540 34. T. Ahmed, S. K. Das, J. K. Golden, E. Saltzman, S. B. Roberts, S. N. Meydani,
541 Calorie restriction enhances T-cell-mediated immune response in adult overweight
542 men and women. *J. Gerontol. A Biol. Sci. Med. Sci.* **64**, 1107–1113 (2009).

543 35. S. Di Biase, C. Lee, S. Brandhorst, B. Manes, R. Buono, C.-W. Cheng, M.
544 Cacciottolo, A. Martin-Montalvo, R. de Cabo, M. Wei, T. E. Morgan, V. D. Longo,
545 Fasting-Mimicking Diet Reduces HO-1 to Promote T Cell-Mediated Tumor
546 Cytotoxicity. *Cancer Cell* **30**, 136–146 (2016).

547 36. R. B. Delconte, M. Owyong, E. K. Santosa, K. Srpan, S. Sheppard, T. J. McGuire,
548 A. Abbasi, C. Diaz-Salazar, J. Chun, I. Rogatsky, K. C. Hsu, S. Jordan, M. Merad,
549 J. C. Sun, Fasting reshapes tissue-specific niches to improve NK cell-mediated
550 anti-tumor immunity. *Immunity*, doi: 10.1016/j.immuni.2024.05.021 (2024).

551 37. B. Homet Moreno, J. M. Zaretsky, A. Garcia-Diaz, J. Tsoi, G. Parisi, L. Robert, K.
552 Meeth, A. Ndoye, M. Bosenberg, A. T. Weeraratna, T. G. Graeber, B. Comin-
553 Anduix, S. Hu-Lieskovan, A. Ribas, Response to programmed cell death-1
554 blockade in a Murine melanoma syngeneic model requires costimulation, CD4, and
555 CD8 T cells. *Cancer Immunol. Res.* **4**, 845–857 (2016).

556 38. G. La Manno, R. Soldatov, A. Zeisel, E. Braun, H. Hochgerner, V. Petukhov, K.
557 Lidschreiber, M. E. Kastriti, P. Lönnerberg, A. Furlan, J. Fan, L. E. Born, Z. Liu, D.
558 van Bruggen, J. Guo, X. He, R. Barker, E. Sundström, G. Castelo-Branco, P.
559 Cramer, I. Adameyko, S. Linnarsson, P. V. Kharchenko, RNA velocity of single
560 cells. *Nature* **560**, 494–498 (2018).

561 39. D. Cheng, K. Qiu, Y. Rao, M. Mao, L. Li, Y. Wang, Y. Song, J. Chen, X. Yi, X.
562 Shao, S. H. Huang, Y. Zhang, X. Chen, S. Wu, S. Yu, J. Liu, H. Wang, X. Peng, D.
563 Li, L. Yang, L. Chen, Z. Ying, Y. Zheng, M. Zheng, B. Ying, X. Zeng, W. Zhang, W.
564 Xu, G. Liu, F. Chen, H. Yu, Y. Zhao, J. Ren, Proliferative exhausted CD8+ T cells
565 exacerbate long-lasting anti-tumor effects in human papillomavirus-positive head
566 and neck squamous cell carcinoma. *Elife* **12**, e82705 (2023).

567 40. K. E. Pauken, M. A. Sammons, P. M. Odorizzi, S. Manne, J. Godec, O. Khan, A. M.
568 Drake, Z. Chen, D. R. Sen, M. Kurachi, R. A. Barnitz, C. Bartman, B. Bengsch, A.
569 C. Huang, J. M. Schenkel, G. Vahedi, W. N. Haining, S. L. Berger, E. J. Wherry,

Epigenetic stability of exhausted T cells limits durability of reinvigoration by PD-1 blockade. *Science* **354**, 1160–1165 (2016).

41. E. H. Ma, M. S. Dahabieh, L. M. DeCamp, I. Kaymak, S. M. Kitchen-Goosen, B. M. Oswald, J. Longo, D. G. Roy, M. J. Verway, R. M. Johnson, B. Samborska, L. R. Duimstra, C. A. Scullion, M. Steadman, M. Vos, T. P. Roddy, C. M. Krawczyk, K. S. Williams, R. D. Sheldon, R. G. Jones, 13C metabolite tracing reveals glutamine and acetate as critical in vivo fuels for CD8 T cells. *Science Advances* **10**, eadj1431 (2024).

42. M. Leney-Greene, A. Boddapati, H. Su, J. Cantor, M. Lenardo, Human plasma-like medium improves T lymphocyte activation. *iScience*, doi: 10.1101/740845 (2019).

43. E. H. Ma, M. J. Verway, R. M. Johnson, D. G. Roy, M. Steadman, S. Hayes, K. S. Williams, R. D. Sheldon, B. Samborska, P. A. Kosinski, H. Kim, T. Griss, B. Faubert, S. A. Condotta, C. M. Krawczyk, R. J. DeBerardinis, K. M. Stewart, M. J. Richer, V. Chubukov, T. P. Roddy, R. G. Jones, Metabolic Profiling Using Stable Isotope Tracing Reveals Distinct Patterns of Glucose Utilization by Physiologically Activated CD8+ T Cells. *Immunity*, doi: 10.1016/j.immuni.2019.09.003 (2019).

44. M. D. Martin, S. A. Condotta, J. T. Harty, V. P. Badovinac, Population dynamics of naive and memory CD8 T cell responses after antigen stimulations in vivo. *J. Immunol.* **188**, 1255–1265 (2012).

45. A. E. Ringel, J. M. Drijvers, G. J. Baker, A. Catozzi, J. C. García-Cañaveras, B. M. Gassaway, B. C. Miller, V. R. Juneja, T. H. Nguyen, S. Joshi, C.-H. Yao, H. Yoon, P. T. Sage, M. W. LaFleur, J. D. Trombley, C. A. Jacobson, Z. Maliga, S. P. Gygi, P. K. Sorger, J. D. Rabinowitz, A. H. Sharpe, M. C. Haigis, Obesity Shapes Metabolism in the Tumor Microenvironment to Suppress Anti-Tumor Immunity. *Cell* **183**, 1848-1866.e26 (2020).

46. S. Hirschberger, L. Gellert, D. Effinger, M. Muenchhoff, M. Herrmann, J.-M. Briegel, B. Zwißler, S. Kreth, Ketone Bodies Improve Human CD8+ Cytotoxic T-Cell Immune Response During COVID-19 Infection. *Front. Med.* **9**, 923502 (2022).

47. P. K. Arnold, B. T. Jackson, K. I. Paras, J. S. Brunner, M. L. Hart, O. J. Newsom, S. P. Alibeckoff, J. Endress, E. Drill, L. B. Sullivan, L. W. S. Finley, A non-canonical tricarboxylic acid cycle underlies cellular identity. *Nature* **603**, 477–481 (2022).

48. M. R. Sullivan, K. R. Mattaini, E. A. Dennstedt, A. A. Nguyen, S. Sivanand, M. F. Reilly, K. Meeth, A. Muir, A. M. Darnell, M. W. Bosenberg, C. A. Lewis, M. G. Vander Heiden, Increased Serine Synthesis Provides an Advantage for Tumors Arising in Tissues Where Serine Levels Are Limiting. *Cell Metab.* **29**, 1410-1421.e4 (2019).

49. I. Kaymak, M. J. Watson, B. M. Oswald, S. Ma, B. K. Johnson, L. M. DeCamp, B. M. Mabvakure, K. M. Luda, E. H. Ma, K. Lau, Z. Fu, B. Muhire, S. M. Kitchen-Goosen, A. Vander Ark, M. S. Dahabieh, B. Samborska, M. Vos, H. Shen, Z. P.

Fan, T. P. Roddy, G. A. Kingsbury, C. M. Sousa, C. M. Krawczyk, K. S. Williams, R. D. Sheldon, S. M. Kaech, D. G. Roy, R. G. Jones, ACLY and ACSS2 link nutrient-dependent chromatin accessibility to CD8 T cell effector responses. *J. Exp. Med.* **221** (2024).

50. W. Bailis, J. A. Shyer, J. Zhao, J. C. G. Canaveras, F. J. Al Khazal, R. Qu, H. R. Steach, P. Bielecki, O. Khan, R. Jackson, Y. Kluger, L. J. Maher 3rd, J. Rabinowitz, J. Craft, R. A. Flavell, Distinct modes of mitochondrial metabolism uncouple T cell differentiation and function. *Nature* **571**, 403–407 (2019).

51. A. Wang, S. C. Huen, H. H. Luan, S. Yu, C. Zhang, J.-D. Gallezot, C. J. Booth, R. Medzhitov, Opposing Effects of Fasting Metabolism on Tissue Tolerance in Bacterial and Viral Inflammation. *Cell* **166**, 1512-1525.e12 (2016).

52. A. Lercher, A. Bhattacharya, A. M. Popa, M. Caldera, M. F. Schlapansky, H. Baazim, B. Agerer, B. Gürtl, L. Kosack, P. Májek, J. S. Brunner, D. Vitko, T. Pinter, J. W. Genger, A. Orlova, N. Pikor, D. Reil, M. Ozsvár-Kozma, U. Kalinke, B. Ludewig, R. Moriggl, K. L. Bennett, J. Menche, P. N. Cheng, G. Schabbauer, M. Trauner, K. Klavins, A. Bergthaler, Type I Interferon Signaling Disrupts the Hepatic Urea Cycle and Alters Systemic Metabolism to Suppress T Cell Function. *Immunity*, doi: 10.1016/j.immuni.2019.10.014 (2019).

53. D. Demiroz, E. Platanitis, M. Bryant, P. Fischer, M. Prchal-Murphy, A. Lercher, C. Lassnig, M. Baccarini, M. Müller, A. Bergthaler, V. Sexl, M. Dolezal, T. Decker, Listeria monocytogenes infection rewires host metabolism with regulatory input from type I interferons. *PLoS Pathog.* **17**, e1009697 (2021).

54. P. Puchalska, P. A. Crawford, Multi-dimensional Roles of Ketone Bodies in Fuel Metabolism, Signaling, and Therapeutics. [Preprint] (2017). https://doi.org/10.1016/j.cmet.2016.12.022.

55. P. Puchalska, P. A. Crawford, Metabolic and Signaling Roles of Ketone Bodies in Health and Disease. *Annu. Rev. Nutr.* **41**, 49–77 (2021).

56. D. J. Drucker, The benefits of GLP-1 drugs beyond obesity. *Science* **385**, 258–260 (2024).

57. O. U. Kawalekar, R. S. O'Connor, J. A. Fraietta, L. Guo, S. E. McGettigan, A. D. Posey Jr, P. R. Patel, S. Guedan, J. Scholler, B. Keith, N. W. Snyder, I. A. Blair, M. C. Milone, C. H. June, Distinct signaling of coreceptors regulates specific metabolism pathways and impacts memory development in CAR T cells. *Immunity* **44**, 380–390 (2016).

58. E. C. Lien, M. G. Vander Heiden, A framework for examining how diet impacts tumour metabolism. *Nat. Rev. Cancer* **19**, 651–661 (2019).

59. J. L. Horton, M. T. Davidson, C. Kurishima, R. B. Vega, J. C. Powers, T. R. Matsuura, C. Petucci, E. D. Lewandowski, P. A. Crawford, D. M. Muoio, F. A.

Recchia, D. P. Kelly, The failing heart utilizes 3-hydroxybutyrate as a metabolic stress defense. *JCI Insight* **4** (2019).

60. D. G. Cotter, R. C. Schugar, A. E. Wentz, D. A. d'Avignon, P. A. Crawford, Successful adaptation to ketosis by mice with tissue-specific deficiency of ketone body oxidation. *Am. J. Physiol. Endocrinol. Metab.* **304**, E363-74 (2013).

61. B. Cordeiro, P. Jeon, G. M. Boukhaled, M. Corrado, O. Lapohos, D. G. Roy, K. Williams, R. G. Jones, S. Gruenheid, S. M. Sagan, C. M. Krawczyk, MicroRNA-9 fine-tunes dendritic cell function by suppressing negative regulators in a cell-type-specific manner. *Cell Rep.* **31**, 107585 (2020).

62. R. D. Sheldon, E. H. Ma, L. M. DeCamp, K. S. Williams, R. G. Jones, Interrogating in vivo T-cell metabolism in mice using stable isotope labeling metabolomics and rapid cell sorting. *Nat. Protoc.*, doi: 10.1038/s41596-021-00586-2 (2021).

63. R. R. J. House, M. T. Soper-Hopper, M. P. Vincent, A. E. Ellis, C. D. Capan, Z. B. Madaj, E. Wolfrum, C. N. Isaguirre, C. D. Castello, A. B. Johnson, M. L. Escobar Galvis, K. S. Williams, H. Lee, R. D. Sheldon, A diverse proteome is present and enzymatically active in metabolite extracts. *Nat. Commun.* **15**, 5796 (2024).

64. E. G. Bligh, W. J. Dyer, A rapid method of total lipid extraction and purification. *Can. J. Biochem. Physiol.*, doi: 10.1139/o59-099 (1959).

65. P. Heinrich, C. Kohler, L. Ellmann, P. Kuerner, R. Spang, P. J. Oefner, K. Dettmer, Correcting for natural isotope abundance and tracer impurity in MS-, MS/MS- and high-resolution-multiple-tracer-data from stable isotope labeling experiments with IsoCorrectoR. *Sci. Rep.* **8**, 17910 (2018).

66. E. E. Vincent, P. P. Coelho, J. Blagih, T. Griss, B. Viollet, R. G. Jones, Differential effects of AMPK agonists on cell growth and metabolism. *Oncogene* **34**, 3627–3639 (2015).

67. S. A. Mookerjee, A. A. Gerencser, D. G. Nicholls, M. D. Brand, Quantifying intracellular rates of glycolytic and oxidative ATP production and consumption using extracellular flux measurements. *J. Biol. Chem.* **292**, 7189–7207 (2017).

68. L. Zhang, Z. Li, K. M. Skrzypczynska, Q. Fang, W. Zhang, S. A. O'Brien, Y. He, L. Wang, Q. Zhang, A. Kim, R. Gao, J. Orf, T. Wang, D. Sawant, J. Kang, D. Bhatt, D. Lu, C.-M. Li, A. S. Rapaport, K. Perez, Y. Ye, S. Wang, X. Hu, X. Ren, W. Ouyang, Z. Shen, J. G. Egen, Z. Zhang, X. Yu, Single-cell analyses inform mechanisms of myeloid-targeted therapies in colon cancer. *Cell* **181**, 442-459.e29 (2020).

69. X. Guo, Y. Zhang, L. Zheng, C. Zheng, J. Song, Q. Zhang, B. Kang, Z. Liu, L. Jin, R. Xing, R. Gao, L. Zhang, M. Dong, X. Hu, X. Ren, D. Kirchhoff, H. G. Roider, T. Yan, Z. Zhang, Global characterization of T cells in non-small-cell lung cancer by single-cell sequencing. *Nat. Med.* **24**, 978–985 (2018).

70. T. S. P. Heng, M. W. Painter, Immunological Genome Project Consortium, The Immunological Genome Project: networks of gene expression in immune cells. *Nat. Immunol.* **9**, 1091–1094 (2008).

71. M. Andreatta, J. Corria-Osorio, S. Müller, R. Cubas, G. Coukos, S. J. Carmona, Interpretation of T cell states from single-cell transcriptomics data using reference atlases. *Nat. Commun.* **12**, 2965 (2021).

72. I. Korsunsky, N. Millard, J. Fan, K. Slowikowski, F. Zhang, K. Wei, Y. Baglaenko, M. Brenner, P.-R. Loh, S. Raychaudhuri, Fast, sensitive and accurate integration of single-cell data with Harmony. *Nat. Methods* **16**, 1289–1296 (2019).

73. L. Zhang, X. Yu, L. Zheng, Y. Zhang, Y. Li, Q. Fang, R. Gao, B. Kang, Q. Zhang, J. Y. Huang, H. Konno, X. Guo, Y. Ye, S. Gao, S. Wang, X. Hu, X. Ren, Z. Shen, W. Ouyang, Z. Zhang, Lineage tracking reveals dynamic relationships of T cells in colorectal cancer. *Nature* **564**, 268–272 (2018).

74. P. Bankhead, M. B. Loughrey, J. A. Fernández, Y. Dombrowski, D. G. McArt, P. D. Dunne, S. McQuaid, R. T. Gray, L. J. Murray, H. G. Coleman, J. A. James, M. Salto-Tellez, P. W. Hamilton, QuPath: Open source software for digital pathology image analysis. *Sci. Rep.* **7**, 16878 (2017).

75. K. Sugawara, Training deep learning models for cell image segmentation with sparse annotations, *bioRxiv* (2023)p. 2023.06.13.544786.

76. A. Kirillov, E. Mintun, N. Ravi, H. Mao, C. Rolland, L. Gustafson, T. Xiao, S. Whitehead, A. C. Berg, W.-Y. Lo, P. Dollár, R. Girshick, Segment Anything, *arXiv [cs.CV]* (2023). http://arxiv.org/abs/2304.02643.

77. C. Stringer, M. Pachitariu, Cellpose3: one-click image restoration for improved cellular segmentation, *bioRxiv* (2024)p. 2024.02.10.579780.

78. M. Pachitariu, C. Stringer, Cellpose 2.0: how to train your own model. *Nat. Methods* **19**, 1634–1641 (2022).

79. C. Stringer, T. Wang, M. Michaelos, M. Pachitariu, Cellpose: a generalist algorithm for cellular segmentation. *Nat. Methods* **18**, 100–106 (2021).

80. J. S. Haring, G. A. Corbin, J. T. Harty, Dynamic regulation of IFN-gamma signaling in antigen-specific CD8+ T cells responding to infection. *J. Immunol.* **174**, 6791–6802 (2005).

Data Availability Statement

All unique and stable reagents generated in this study are available from the Lead Contact upon completion of a Materials Transfer Agreement. CITE-sequencing data of mouse tumor-infiltrating lymphocytes have been deposited in the National Center for Biotechnology Information Gene Expression Omnibus (NCBI GEO) under accession number GSE267070. Human single-cell RNA-sequencing data of tumor-infiltrating

762 lymphocytes used in this research are available at NCBI GEO under accession number

763 GSE146771. All other data supporting the findings of this study are available within the

764 article and its online supplementary material. Bioenergetics data were analyzed using

765 protocols developed by Mookerjee and Brand, available for download at

766 https://russelljoneslab.vai.org. R code used for data processing is available at our

767 GitHub repository (https://github.com/rgjcanada/DR_CITESEQ_2025.git). Processed

768 data files (RDS files) curated from the data processing can be found at

769 https://doi.org/10.5281/zenodo.13920173.

770

771 **Supplementary Materials**

772 Materials and Methods

773 Figs. S1 to S10

774 Tables S1 to S8

775

776

Figure Legends

Figure. 1. Dietary restriction enhances T cell-mediated anti-tumor immunity.
A) Schematic representation of dietary interventions and tumor experiment design.
B) Daily food intake (grams) of mice on *ad libitum* (AL) or dietary restriction (DR) feeding regimens. Data represent the mean $\pm$ SEM (n = 6 mice/group).
C) Weight loss (% change from baseline) of mice after 1 week of feeding on AL or DR diets. Data represents the mean $\pm$ SEM (2 weeks, n = 12 mice/group).
D-E) Growth of (D) B16 melanoma or (E) EO771 breast cancer cells in C57BL/6 mice fed an AL or DR diet. *Left,* Kaplan-Meier plots comparing tumor onset (tumor volume ≥250 mm³) between AL and DR groups. *Right*, spaghetti plots of individual tumor volumes growth curves over time. The darker lines indicate the average tumor growth for each diet group over time post tumor injection (PTI). B16, n=16-20 mice/group; EO771, n=15 mice/group. Statistical significance was assessed by long-rank test.
F) Kaplan-Meier plot comparing tumor onset in B16 tumor-bearing wild-type (WT) and *Rag2*$^{-/-}$ mice on an AL or DR diet. Statistical significance was assessed by log-rank test (n=5 mice/group).
G) Kaplan-Meier plot comparing time-to-humane endpoint in CD8$^+$ T cell-depleted mice fed an AL and DR diet. Mice were treated with control (IgG) or CD8$^+$ T cell depleting (Anti-CD8) antibodies prior to tumor cell implantation. Statistical significance was assessed by log-rank test (n = 4-8 mice/group, endpoint = 1500mm^3).
H) Weighted nearest neighbor Uniform Manifold Approximation and Projection (wnnUMAP) of 45,455 CD45$^+$ tumor-infiltrating cells (AL and DR combined) from B16 melanoma tumors (*left*; n = 4 mice/diet). *Right,* Breakdown of immune cell populations from all CD45$^+$ cells (top) or CD3$^+$ T cells (bottom).
I) Histology of B16 tumors from AL- or DR-fed 14 days post tumor implantation. *Left,* immunohistochemical staining for CD8$^+$ T cells and H&E staining of representative tumor sections. *Right,* quantification of positive CD8$^+$ staining per tumor section (DAB/mm^2). Data represent the mean $\pm$ SEM (n = 3 mice/group).
J) Kaplan-Meier plot comparing B16 melanoma tumor onset in AL- or DR-fed mice that received anti-PD1 or IgG control antibodies by i.p. injection (200 μg/dose). Antibody treatment was administered every 3 days for a total of 5 injections, beginning 7 days PTI (n = 11-20 mice/group). Statistical significance was assessed by log-rank test with Bonferroni correction.
*P<0.05, **P<0.01, ***P<0.001, ****P<0.0001.

Fig. 2. Dietary restriction reduces T cell dysfunction in the tumor microenvironment.
A) Weighted nearest neighbor UMAP (wnnUMAP) of 7,005 activated (CD44$^+$) CD8$^+$ tumor-infiltrating lymphocytes (TILs) from B16 melanoma tumors (combined AL and DR) (n = 4). Legend indicates unique T cell clusters called based on RNA expression and antibody-derived tags (ADTs). T cell clusters with high and low *Tox* expression are highlighted by circles.
B) Overlay of wnnUMAP for activated CD8$^+$ TIL from (A) and MSigDB gene expression signatures for effector-like Tex cells (Tex^{Eff}), Cell Cycle, and GO Immune Response pathways for TILs isolated from B16 tumors (combined AL and DR). Joint density plot

823   indicates the highest combined expression/cell of *Ifng*, *Tnfa*, and *Gzmb* among
824   activated CD8+ T cells from B16 tumors.
825   C) wnnUMAP of activated CD8+ TILs divided by dietary conditions (AL: 3,348 cells, DR:
826   3,657 cells). Prominent CD8+ T cell clusters are indicated.
827   D) Stacked bar graphs showing the percentage of CD8+ T cell populations divided by
828   *Tox* expression (*Tox*Low versus *Tox*High).
829   E) RNA velocity plots inferring cellular differentiation trajectory for CD8+ T cells
830   infiltrating B16 tumors from AL- or DR-fed mice. Trajectories were derived from the
831   dynamical prediction model scVelo, with representative directionality for T cells under
832   each diet shown in inset.
833   F) PD1 and TOX expression in B16 tumor-infiltrating CD8+ T cells isolated from AL or
834   DR mice 14 days PTI. *Top*, representative flow cytometry plots for PD1 versus TOX
835   expression. *Bottom*, bar graphs showing the percentage of PD1+TOX+ and PD1+TIM3+
836   CD8+ T cells isolated from tumors. Data represents the mean ± SEM (n = 8 mice/group).
837   G) Expression of stemness, exhaustion, and effector molecules in TOX+ CD8+ T cells
838   isolated from B16 tumors from AL- or DR-fed mice. *Top*, representative histograms of
839   LY108, PD1, TOX, and GZMB expression. Geometric mean fluorescence intensity
840   (gMFI) averaged across all biological replicates is indicated in inset. *Bottom*, bar graphs
841   quantifying the percentage of CD8+ cells expressing each of the indicated proteins. Data
842   represent the mean ± SEM (n = 7-8 mice/group).
843   H) PD1 and TOX expression in B16 tumor-infiltrating CD8+ T cells from DR-fed mice
844   treated with anti-PD1 immunotherapy. DR-fed mice harboring B16 tumors were
845   administered anti-IgG or anti-PD1 antibodies (200 ug i.p.) every 3 days for 5 doses,
846   beginning on day 7 PTI. CD8+ T cells were isolated from B16 melanoma tumors at 21
847   days PTI. *Left*, representative flow cytometry plots for TOX versus PD1 expression.
848   *Right*, bar graph showing the percentage of PD1+TOX+ CD8+ T cells following IgG or
849   anti-PD1 treatment. Data represent the mean ± SEM (n = 8 mice/group.
850   I) Bar graphs quantifying the percentage of TOX+ CD8+ T cells expressing high levels of
851   TOX (TOXHigh), both IFN-γ and TNF-α (IFNG+TNFA+), and GZMB following IgG or anti-
852   PD1 treatment from (H). Data represent the mean ± SEM (n = 8 mice/group).
853   *P<0.05, **P<0.01, ***P<0.001, ****P<0.0001.
854
855   **Fig. 3. Dietary restriction enhances CD8+ T cell metabolic fitness via enhanced**
856   **ketone body metabolism.**
857   A) Overlay of wnnUMAP for 7,005 activated (CD44+) CD8+ TIL from B16 melanoma
858   tumors (both AL and DR) and MSigDB gene expression signatures for organic oxidation
859   and glycolysis pathways.
860   B-C) Bioenergetic profile of AL- and DR-conditioned CD8+ T cells. (B) Oxygen
861   consumption rate (OCR) plot for antigen-specific CD8+ T cells isolated from *Lm*OVA-
862   infected AL- or DR-fed mice (7 days post infection (dpi)). Data represent the mean ± SD
863   (n = 24-46, technical replicates). Oligomycin (Oligo), FCCP, rotenone and antimycin A
864   (Rot/AA), and monensin (Mon) were added to cells where indicated. C) Basal and
865   maximal ATP production rates from OXPHOS for AL- or DR-conditioned CD8+ T cells
866   from (B). Data represent the mean ± SD (n = 24-46, technical replicates).
867   D) The relative abundance (Z-score) of TCA cycle-derived metabolites in antigen-specific
868   CD8+ T cells isolated from *Lm*OVA-infected AL- or DR-fed mice 7 dpi (n=3 mice/group).

869   E) Mitochondrial membrane potential of AL- and DR-conditioned CD8$^+$ T cells. *Left,*
870   TMRM staining (gMFI) of CD8$^+$ OT-I TIL isolated from B16 tumors from AL- or DR-fed
871   mice (14 days PTI). *Right*, TMRM staining of CD8$^+$ OT-I T cells isolated from the spleen
872   of *Lm*OVA-infected AL- or DR-fed mice (7 dpi). Data represent the mean $\pm$ SEM (n = 4
873   mice/group).
874   F) Volcano plot showing the log$_2$ fold change in metabolite and lipid abundance in B16
875   tumors isolated from AL versus DR mice (n = 3-4 mice/group). Select metabolites
876   enriched in AL and DR tumors are annotated.
877   G) Ketone body levels in the serum and tumors of AL- versus DR-fed mice after 21 days
878   on diet (14 days of tumor growth). *Left,* βOHB abundance in B16 tumors from AL- versus
879   DR-fed mice as quantified by mass spectrometry. *Right*, Ketone body abundance in
880   serum as quantified by enzyme assay. Data represent the mean $\pm$ SEM (n=3-4
881   mice/group).
882   H-I) Bioenergetic profile of AL- and DR-conditioned CD8$^+$ T cells exposed to βOHB. (H)
883   OCR plot for antigen-specific CD8$^+$ T cells isolated from *Lm*OVA-infected AL- or DR-fed
884   mice (7 dpi). T cells were cultured with or without 1.5 mM βOHB 60 minutes prior to the
885   start of the assay. I) Maximum ATP production rates from OXPHOS for CD8$^+$ T cells from
886   (H). Data represent the mean $\pm$ SD (n = 8-16, technical replicates).
887   J) Schematic depicting ^{13}C labeling patterns in acetyl-CoA (Ac-CoA) and TCA cycle
888   intermediates from U-[^{13}C$_6$]-glucose and [2,4-^{13}C$_2$]-βOHB.
889   K-M) ^{13}C labeling of TCA cycle intermediates in AL- versus DR-conditioned CD8$^+$ T cells.
890   CD8$^+$ T cells isolated from *Lm*OVA-infected AL- or DR-fed mice (7 dpi) were cultured for
891   2h *ex vivo* in VIM medium containing 5 mM U-[^{13}C$_6$]-glucose and 1.5 mM [2,4-^{13}C$_2$]-βOHB.
892   Shown is the percent incorporation of (K) U-[^{13}C$_6$]-glucose-derived carbon (M+2) and (L)
893   [2,4-^{13}C$_2$]-βOHB-derived carbon (M+1) into citrate and malate. M) Ratio of [2,4-^{13}C$_2$]-
894   βOHB-labeled malate (M+1) to citrate (M+1) for T cells from panel (L). Data represent the
895   mean $\pm$ SEM (n = 3 mice/group).
896   N) Bar graph of Ac-CoA abundance in CD8$^+$ T cells isolated from *Lm*OVA-infected AL- or
897   DR-fed mice (7 dpi). Data represent the mean $\pm$ SEM (n = 12 mice/group).
898   *P<0.05, **P<0.01, ***P<0.001, ****P<0.0001.
899
900   **Fig. 4. Ketone bodies fuel anti-tumor immunity under dietary restriction.**
901   A) Uniform Manifold Approximation and Projection (UMAP) of 8,552 cells human CD8$^+$
902   tumor-infiltrating lymphocytes (TILs) from GSE98638. Shown are unique clusters for
903   effector (Teff), memory (Tmem), terminally exhausted (Tex^{Term}), and proliferating
904   exhausted (Tex^{Eff}) CD8$^+$ T cell populations.
905   B-C) Violin plots of gene expression across human CD8$^+$ TIL subsets. B) Expression of
906   *BDH1*, and *OXCT1* genes. C) Expression of ketolysis signature genes (Ketolysis gene
907   set: *ACAT1, ACAT2, BDH1, BDH2, HMGCL, HMGCS1, HMGCS2, OXCT1, OXCT2*).
908   Statistical significance was assessed by one-way ANOVA with Dunnett's multiple
909   comparisons test and a 5% significance level.
910   D) Heatmap showing the relative abundance (Z-score) of TCA cycle-derived
911   metabolites from CD8$^+$ T cells exposed to acute versus chronic stimulation with anti-
912   CD3 and -CD28 antibodies *in vitro* (n = 3 mice/group).
913   E) Bar graph depicting total abundance of ^{13}C-labeled βOHB in acute versus chronic
914   stimulated CD8$^+$ T cells as in (D). Data represent the mean $\pm$ SEM (n = 3 mice/group).

915   F-G) ^{13}C labeling of TCA cycle intermediates in CD8$^+$ T cells exposed to chronic antigen
916   stimulation. CD8$^+$ T cells exposed to acute versus chronic stimulation as in (D) were
917   cultured in VIM medium containing 0.85 mM [^{13}C$_4$]-βOHB for 2h. F) Total abundance of
918   [^{13}C4]-βOHB-derived citrate and malate. G) Ratio of [^{13}C$_4$]-βOHB-labeled malate (M+2)
919   to citrate (M+2) for T cells from (F). Data represent the mean ± SEM (n = 3 mice/
920   group).
921   H) Immunoblot of SCOT and BDH1 protein expression in CD8$^+$ T cells from wild type
922   (WT, *Cd4-Cre$^-$*; *Bdh1$^{fl/fl}$Oxct1$^{fl/fl}$*) or *Bdh1/Oxct1* double knockout (DKO, *Cd4-Cre$^+$*;
923   *Bdh1$^{fl/fl}$Oxct1$^{fl/fl}$*). Protein levels of α-tubulin are shown as a loading control.
924   I) Bioenergetic profile of control (WT) and ketolysis-deficient (DKO) CD8$^+$ T cells under
925   DR conditions. *Left,* OCR plot of WT and DKO OT-I T cells isolated from DR-fed
926   *Lm*OVA-infected mice (7 dpi). *Right*, bar graph showing maximal ATP production rates
927   from OXPHOS for WT versus DKO CD8$^+$ T cells. Data represent the mean ± SM (n=19-
928   20).
929   J) ^{13}C labeling of TCA cycle intermediates in control (WT) and ketolysis-deficient (DKO)
930   CD8$^+$ T cells under DR conditions. Bar graph showing U-[^{13}C4]-βOHB labeling in citrate
931   M+2 (*left*) and malate M+2(*right*) in WT versus DKO CD8$^+$ T cells isolated from DR-fed
932   *Lm*OVA-infected mice (7 dpi). Data represent the mean ± SEM (n = 4 mice/group).
933   K) Mitochondrial membrane potential of control (WT) versus ketolysis-deficient (DKO)
934   CD8$^+$ T cells under DR conditions. Bar plot showing TMRM staining of CD8$^+$ T cells
935   isolated from *Lm*OVA-infected AL- or DR-fed mice (7 dpi). Data represent the mean ±
936   SEM (n = 4 mice/group).
937   L) Kaplan-Meier plot comparing tumor onset (tumor volume ≥250 mm^3) in B16 tumor-
938   bearing WT versus DKO mice fed an AL or DR diet as in Figure 1D. Statistical
939   significance was assessed by log-rank test with Bonferroni correction (n=16-19
940   mice/group).
941   M-N) Enhanced exhaustion of DKO CD8$^+$ T cells under DR-fed conditions. (M) Bar plot
942   showing the percentage of PD1$^+$TOX$^+$ CD8$^+$ T cells isolated from B16 tumors from WT
943   versus DKO mice under AL- or DR-fed conditions. N) Representative histograms of
944   TOX expression in CD8$^+$ TIL isolated from B16 tumors from WT and DKO mice fed
945   under AL- or DR-conditions. *Inset,* gMFI values for TOX expression averaged across all
946   biological replicates. Data represent the mean ± SEM (n = 8-10).
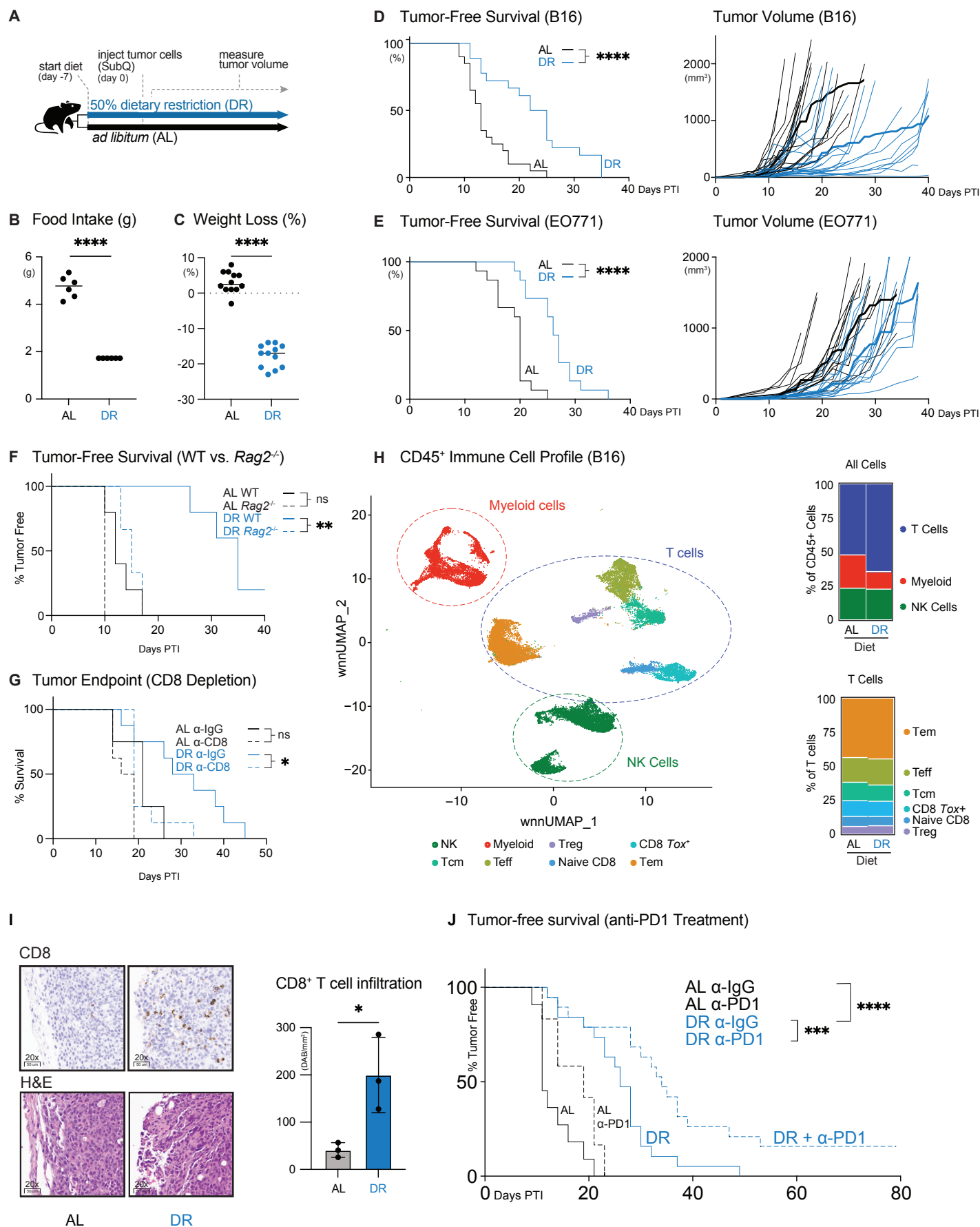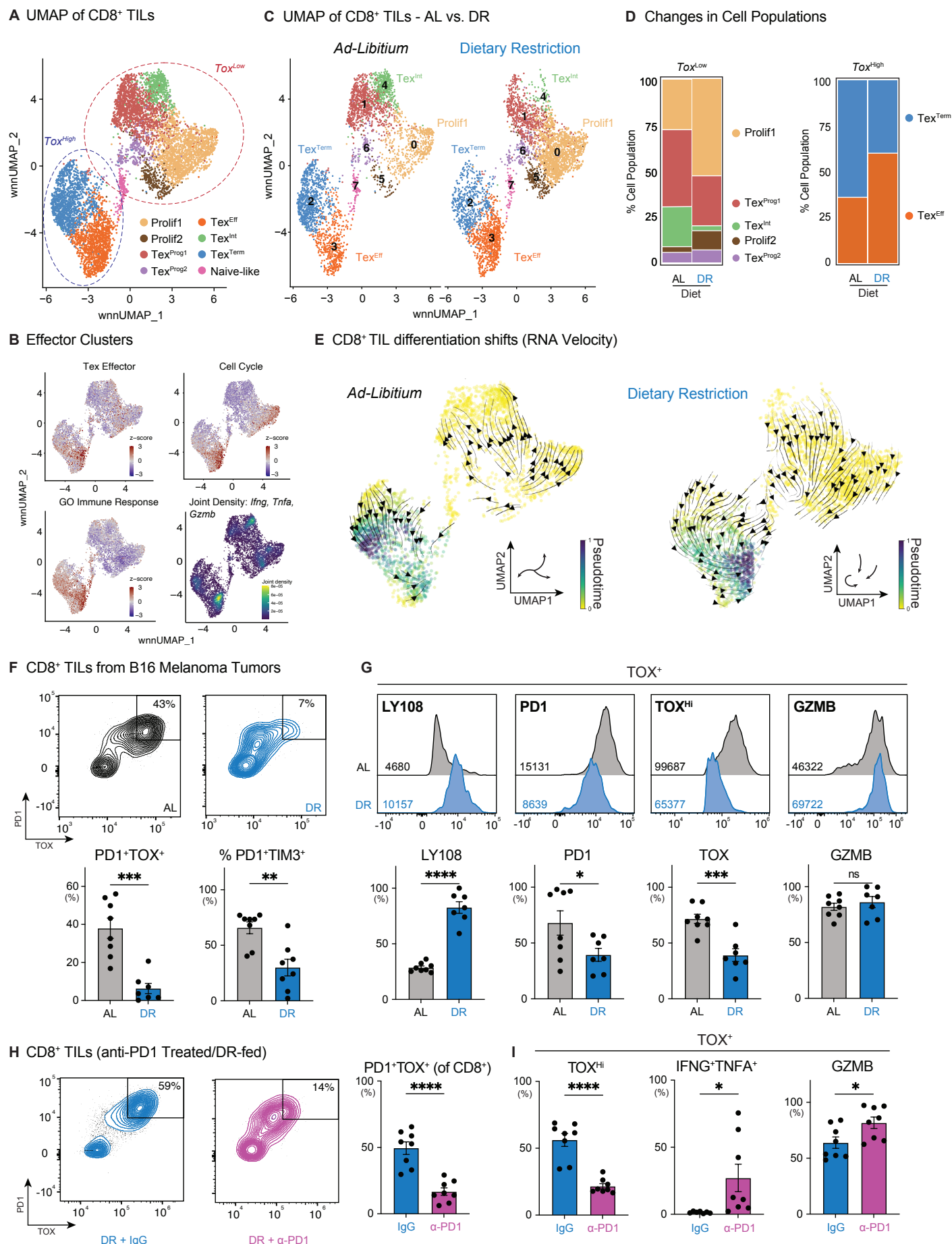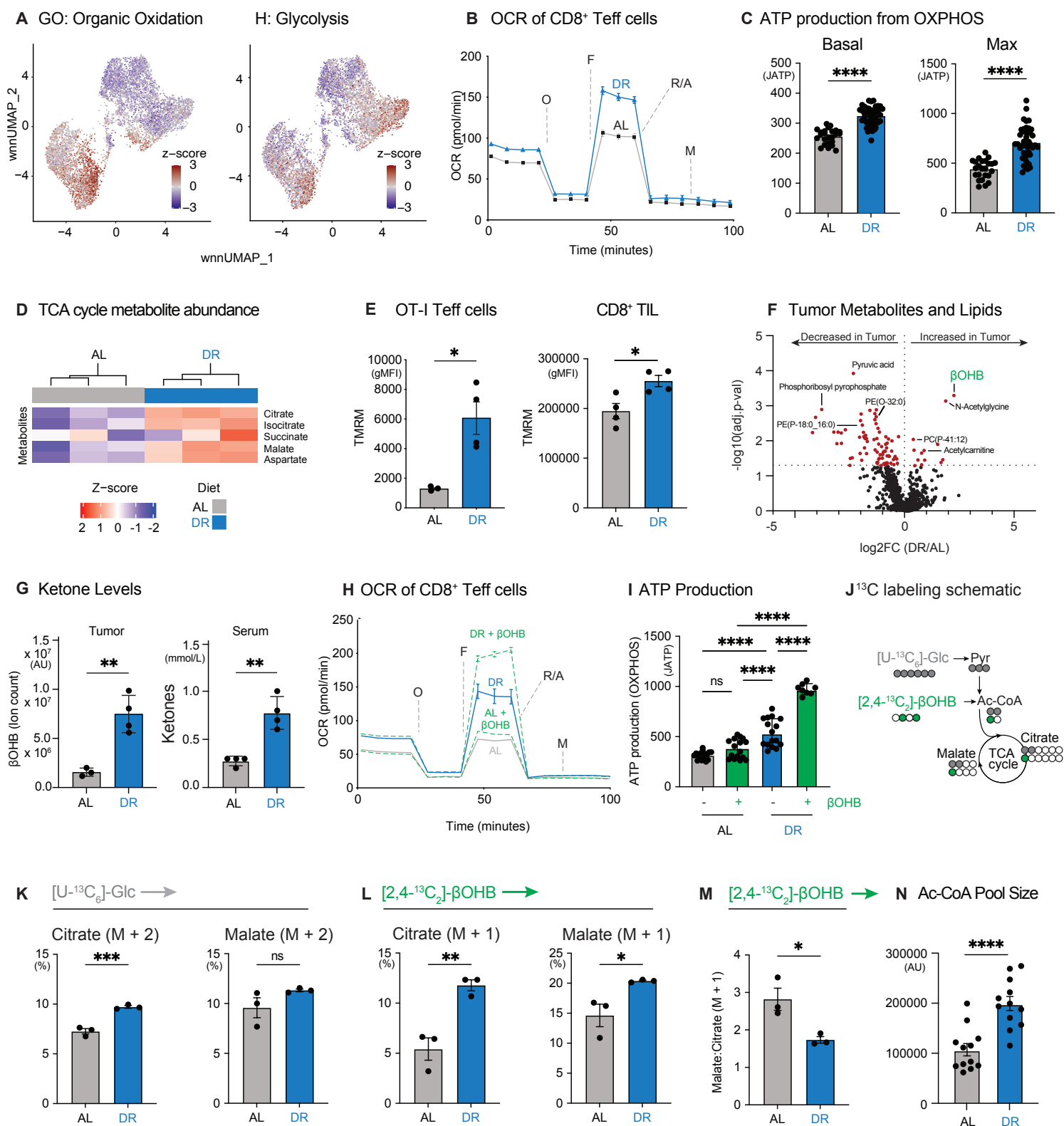947   *P<0.05, **P<0.01, ***P<0.001, ****P<0.0001.

Figure 1

Figure 2

A UMAP of CD8⁺ TILs

B Effector Clusters

C UMAP of CD8⁺ TILs - AL vs. DR

D Changes in Cell Populations

E CD8⁺ TIL differentiation shifts (RNA Velocity)

F CD8⁺ TILs from B16 Melanoma Tumors

G TOX⁺

H CD8⁺ TILs (anti-PD1 Treated/DR-fed)

I TOX⁺

Figure 3

Figure 4